Research Square

Preprints are preliminary reports that have not undergone peer review.
They should not be considered conclusive, used to inform clinical practice,
or referenced by the media as validated information.

# SWI/SNF ATPase degradation suppresses hepatocellular carcinoma growth in part through PLAU transcriptional repression

**Kohichi Takada**

ktakada@sapmed.ac.jp

Sapporo Medical University School of Medicine https://orcid.org/0000-0002-1393-9442

**Norito Suzuki**

https://orcid.org/0000-0001-9119-5883

**Yutaka Kawano**

Sapporo medical university

**Tomohiro Kubo**

**Yohei Arihara**

**Terufumi Kubo**

**Yutaka Okagawa**

**Masahiro Hirakawa**

**Ryota Yokoyama**

**Hayato Watabe**

**Seiyu Kubota**

**Reo Maruyama**

Japanese Foundation for Cancer Research https://orcid.org/0000-0001-7166-5964

**Article**

**Keywords:**

**Posted Date:** November 20th, 2026

**DOI:** https://doi.org/10.21203/rs.3.rs-11524824/v1

**License:** This work is licensed under a Creative Commons Attribution 4.0 International License.
Read Full License

**Additional Declarations: Yes** there is potential conflict of interest.

# SWI/SNF ATPase degradation suppresses hepatocellular carcinoma growth in part through *PLAU* transcriptional repression

Norito Suzuki[1*], Yutaka Kawano[1*], Tomohiro Kubo[1], Yohei Arihara[1], Terufumi Kubo[2], Yutaka Okagawa[1], Masahiro Hirakawa[1], Ryota Yokoyama[1], Hayato Watabe[1], Seiyu Kubota[1], Reo Maruyama[3], and Kohichi Takada[1]

[1] Division of Medical Oncology, Department of Internal Medicine, Sapporo Medical University School of Medicine, Sapporo, Japan

[2] Department of Pathology, Sapporo Medical University School of Medicine, Sapporo, Japan

[3] Division of Cancer Epigenomics, Cancer Institute, Japanese Foundation for Cancer Research, Tokyo, Japan.

[*] Norito Suzuki and Yutaka Kawano equally contributed this work.

Correspondence to: Kohichi Takada, Division of Medical Oncology, Department of Internal Medicine, Sapporo Medical University School of Medicine, South 1, West 16, Chuo-ku, Sapporo, Hokkaido, 060-8543, Japan

Email: ktakada@sapmed.ac.jp

Telephone number: +81-11-611-2111 (ext 32540)

**Abstract**

The SWItch/sucrose non-fermentable (SWI/SNF) chromatin-remodelling complex regulates transcriptional programs involved in cancer progression; however, the therapeutic relevance of SWI/SNF ATPase degradation in hepatocellular carcinoma remains unclear. We assessed the antitumour activity and downstream transcriptional effects of AU-15330, a proteolysis-targeting chimera that degrades the SWI/SNF ATPases, such as SWI/SNF-related, matrix-associated, actin-dependent regulator of chromatin, subfamily A (SMARCA)2 and SMARCA4. In The Cancer Genome Atlas Liver Hepatocellular Carcinoma cohort, high *SMARCA4* expression was associated with shorter overall survival. AU-15330 reduced SMARCA2 and SMARCA4 protein levels, decreased hepatocellular carcinoma cell viability, induced apoptosis, and suppressed tumour growth in a Hep3B xenograft model. RNA sequencing identified *plasminogen activator, urokinase (PLAU)* as a candidate downstream effector, and AU-15330 rapidly suppressed *PLAU* expression and urokinase-type plasminogen activator secretion. Additionally, AU-15330 reduced c-Jun occupancy and H3K27ac enrichment at upstream *PLAU* enhancer regions without significantly altering c-Jun abundance or Ser73 phosphorylation. Moreover, *PLAU* overexpression partially attenuated AU-15330-induced growth inhibition. These findings indicate that *PLAU* repression partly

contributes to the antitumour effects of SWI/SNF ATPase degradation in hepatocellular carcinoma and support further assessment of this transcriptional dependency.

## Introduction

Hepatocellular carcinoma (HCC) remains a major global health burden and leading cause of cancer-related mortality worldwide (1). Although viral hepatitis has historically been a major driver of HCC, alcohol-associated liver disease and metabolic dysfunction-associated steatotic liver disease are becoming increasingly crucial aetiologies (2). Systemic treatment for advanced HCC has evolved from multikinase inhibitors, including sorafenib (3) and lenvatinib (4) to immune-based regimens, such as atezolizumab plus bevacizumab (5), tremelimumab plus durvalumab (6), and nivolumab plus ipilimumab (7). However, durable disease control remains limited for many patients, highlighting the need to identify additional therapeutically actionable molecular vulnerabilities.

Epigenetic dysregulation is increasingly recognised as a primary determinant of cancer cell identity, transcriptional dependency, and therapeutic vulnerability (8, 9). The SWItch/sucrose non-fermentable (SWI/SNF) chromatin-remodelling complex uses

ATP-dependent nucleosome remodelling to regulate chromatin accessibility and transcription factor engagement at regulatory elements, thereby shaping cancer-related transcriptional programs (10). SWI/SNF subunits are recurrently altered across human cancers (11), and alterations in SWI/SNF-related, matrix-associated, actin-dependent regulator of chromatin, subfamily A (SMARCA)4 that encodes the Brahma-related gene 1 catalytic ATPase subunit, have been observed across multiple tumour types (12). Notably, targeted degradation of the SWI/SNF ATPases SMARCA2 and SMARCA4 by the proteolysis-targeting chimera AU-15330 disrupts enhancer-dependent oncogenic transcription and suppresses tumour growth in enhancer-addicted prostate cancer models (13). However, whether SWI/SNF ATPase degradation exerts antitumour activity in HCC and which downstream transcriptional programs mediate such effects remain unclear.

In this study, we assessed the antitumour activity of SWI/SNF ATPase degradation in HCC and aimed to define the transcriptional mechanisms underlying its effect. Using HCC cell models, a Hep3B xenograft model, transcriptomic profiling, and chromatin immunoprecipitation analyses, we observed that AU-15330 suppressed HCC growth and repressed *plasminogen activator, urokinase (PLAU)* expression. AU-15330 reduced c-Jun occupancy and H3K27ac enrichment at the upstream *PLAU* enhancer regions,

whereas forced *PLAU* expression partially attenuated AU-15330-induced growth inhibition. These findings identify *PLAU* repression as a functionally relevant downstream consequence of SWI/SNF ATPase degradation and support further assessment of this strategy in HCC.

## Materials and Methods

### Reagents

AU-15330, a proteolysis-targeting chimera degrader targeting SMARCA2 and SMARCA4, was purchased from Selleck Biotechnology (Yokohama, Japan). AU-15330 was dissolved in dimethyl sulfoxide (DMSO; Sigma-Aldrich, St. Louis, MO, USA) to prepare a 10 mM stock solution. For in vitro experiments, the stock solution was diluted in the culture medium immediately before use, and DMSO-treated cells served as vehicle controls.

### Cell lines and culture conditions

Hep3B cells were obtained from the American Type Culture Collection (Manassas, VA, USA). HuH-7 and JHH-6 cells were obtained from the Japanese Collection of Research

Bioresources Cell Bank (JCRB, Osaka, Japan). The cells were cultured in Dulbecco's modified Eagle's medium (Gibco, Thermo Fisher Scientific, Waltham, MA, USA) supplemented with 10 % foetal bovine serum (Sigma-Aldrich), 10 mM L-glutamine, 100 U/mL penicillin, and 100 μg/mL streptomycin and maintained at 37 °C in a humidified atmosphere containing 5 % $CO_2$. Unless otherwise indicated, mechanistic experiments were primarily performed in Hep3B cells, with selected findings independently assessed in HuH-7 cells.

**Analysis of public HCC transcriptome data**

Gene expression and clinical data were obtained from The Cancer Genome Atlas Liver Hepatocellular Carcinoma (TCGA-LIHC) cohort. Expression levels of *SMARCA2*, *SMARCA4*, and polybromo-1 (*PBRM1*) were compared between HCC and matched adjacent non-tumour liver tissues. Paired tumour and adjacent non-tumour samples were compared using the Wilcoxon signed-rank test. For survival analysis, patients in the upper (75th–100th percentile) and lower (0–25th percentile) quartiles of expression for each gene were compared. Overall survival was estimated using the Kaplan–Meier method, and differences between groups were assessed using the log-rank test. Statistical analyses were performed using EZR version 1.65 (14).

## Cell viability assay

Cell viability was assessed using the CellTiter-Glo 2.0 Assay (Promega, Madison, WI, USA). Hep3B, HuH-7, and JHH-6 cells were seeded in 96-well plates at 5,000 cells per well and incubated overnight. Subsequently, the cells were treated with AU-15330 at concentrations ranging from 0.1–100 μM or with vehicle for 48 h. Luminescence was measured using a GloMax Explorer microplate reader (Promega) and normalized to the corresponding vehicle-treated controls. Half-maximal inhibitory concentration ($IC_{50}$) values were estimated by nonlinear regression using GraphPad Prism version 11 (GraphPad Software, Boston, MA, USA).

## Western blotting

The cells were lysed in radioimmunoprecipitation assay buffer (Nacalai Tesque, Kyoto, Japan) supplemented with Halt Protease and Phosphatase Inhibitor Cocktail (Thermo Fisher Scientific). Protein concentrations were determined using the Pierce bicinchoninic acid assay Protein Assay Kit (Thermo Fisher Scientific). Protein lysates (20–50 μg) were separated on 4–20 % Mini-PROTEAN TGX gels (Bio-Rad Laboratories, Hercules, CA, USA) and transferred onto polyvinylidene difluoride membranes using a QBlot kit M

(ATTO, Tokyo, Japan). The membranes were blocked with 5 % nonfat dry milk and incubated overnight at 4 °C with primary antibodies against Brahma-related gene 1 (#49360; 1:1000), BRM (#11966; 1:1000), PBRM1 (#91894; 1:1000), poly (ADP-ribose) polymerase (PARP) (#9532; 1:1000), cleaved PARP (#9541; 1:1000), urokinase-type plasminogen activator (uPA) (#15800; 1:1000), c-Jun (#9165; 1:1000), phospho-c-Jun (Ser73; #9164; 1:1000), or green fluorescent protein (GFP) (#2956; 1:1000), all from Cell Signaling Technology (Danvers, MA, USA), or with horseradish peroxidase-conjugated β-actin antibody (sc-1615; Santa Cruz Biotechnology, Dallas, TX, USA). After washing, the membranes were incubated with horseradish peroxidase-conjugated secondary antibody (#7074; 1:2000; Cell Signaling Technology). Protein bands were visualised using Amersham ECL Prime Western Blotting Detection Reagent (Cytiva, Marlborough, MA, USA) and a WSE-6100 LuminoGraph I system (ATTO). Band intensities were quantified using the ImageJ version 1.53 and normalised to β-actin.

**Quantitative reverse transcription-polymerase chain reaction (qRT-PCR)**

Total RNA was extracted using TRIzol reagent (Thermo Fisher Scientific), and 1 μg of total RNA was reverse-transcribed using the SuperScript VILO cDNA Synthesis Kit (Thermo Fisher Scientific). Quantitative real-time PCR was performed using PowerUp

SYBR Green Master Mix (Thermo Fisher Scientific) on a QuantStudio 3 Real-Time PCR System (Thermo Fisher Scientific). Relative mRNA expression was calculated using the 2^−ΔΔCt method, with beta-actin as the reference gene. The primer sequences were as follows: *beta-actin*, forward 5′-GGCATCCTCACCCTGAAGTA-3′ and reverse 5′-CCATCTCTTGCTCGAAGTCC-3′; *SMARCA4*, forward 5′-GACCAGCACTCCCAAGGTTAC-3′ and reverse 5′-CTGGCCCGGAAGACATCTG-3′; *SMARCA2*, forward 5′-AGCGGGAATACAGACTTCAGG-3′ and reverse 5′-AAGTGCTTTTAGTTCCACGGTT-3′; *PBRM1*, forward 5′-AGGAGGAGACTTTCCAATCTTCC-3′ and reverse 5′-CTTCGCTTTGGTGCCCTAATG-3′; and *PLAU*, forward 5′-GGGAATGGTCACTTTTACCGAG-3′ and reverse 5′-GGGCATGGTACGTTTGCTG-3′.

**Flow cytometry**

Apoptosis was assessed using the phycoerythrin Annexin V Apoptosis Detection Kit I (BD Biosciences, Franklin Lakes, NJ, USA). Cells were seeded at 2 × 10^5 cells per well in 6-well plates and treated with AU-15330 or vehicle for 48 h. AU-15330 was used at 6, 12, and 18 μM for Hep3B cells and at 12, 24, and 36 μM for HuH-7 cells.

Both floating and adherent cells were collected and stained with phycoerythrin-conjugated Annexin V and 7-aminoactinomycin D (7-AAD), following the manufacturer's protocol. Samples were analysed using a FACSCanto II flow cytometer (BD Biosciences), and data were analysed using FlowJo software (Tree Star Inc., Ashland, OR, USA). Total apoptotic cells were defined as the sum of early (Annexin $V^+/7\text{-}AAD^-$) and late (Annexin $V^+/7\text{-}AAD^+$) apoptotic populations.

**Time-course apoptosis assay**

Time-dependent apoptosis was assessed using the RealTime-Glo™ Annexin V Apoptosis Assay (Promega). Hep3B cells were seeded at 10,000 cells per well in white 96-well plates and treated with 6, 12, or 18 μM AU-15330, vehicle, or 1 μM staurosporine as a positive control. Luminescence was measured at 0, 1, 3, 6, 12, 15, 18, and 24 h after treatment using a GloMax Explorer microplate reader (Promega). Apoptosis-associated luminescence was corrected by subtracting the corresponding value from vehicle-treated cells at each time point.

**RNA sequencing and differential expression analysis**

Hep3B cells were treated with 12 μM AU-15330 or DMSO for 6 or 12 h. Total RNA was extracted using TRIzol reagent. Poly(A)-selected libraries were prepared using the NEBNext Poly(A) mRNA Magnetic Isolation Module and NEBNext Ultra II Directional RNA Library Prep Kit (New England Biolabs, Ipswich, MA, USA). Libraries were sequenced on an Illumina NovaSeq X Plus platform using 150-bp paired-end reads, yielding approximately 20 million read pairs per sample. RNA sequencing was performed using two biological replicates per condition. Read quality was assessed using FastQC (version 0.12.1), and adapter sequences and low-quality reads were removed using Trimmomatic (version 0.38). Reads were aligned to the human GRCh38 reference genome using HISAT2 (version 2.1.0), and gene-level counts were generated using featureCounts (version 1.6.3). Differential expression analysis was performed using DESeq2 (version 1.24.0) with Benjamini–Hochberg correction for multiple testing. Genes with adjusted P value < 0.01 and absolute $\log_2$ fold change > 2 were considered differentially expressed. Venn diagrams were generated using InteractiVenn (15). The RNA-sequencing data were deposited in the DNA Data Bank of Japan Sequenced Read Archive under accession number DRR1093361-DRR1093370.

**Measurement of uPA secretion using enzyme-linked immunosorbent assay**

**(ELISA)**

Secreted uPA was quantified in culture supernatants using the Human u-Plasminogen Activator/Urokinase Quantikine ELISA Kit (R&D Systems, Minneapolis, MN, USA). Cells were seeded at 2.0 × 10^5 cells per well and treated with AU-15330 or DMSO for 3, 6, or 12 h. AU-15330 was used at 12 μM for Hep3B cells and 24 μM for HuH-7 cells. Culture supernatants were collected at each time point, and uPA concentrations were measured following the manufacturer's protocol. Additionally, uPA concentrations were measured in the culture supernatants of Hep3B cells overexpressing *PLAU* and control cells.

**Chromatin immunoprecipitation–quantitative PCR (ChIP-qPCR)**

ChIP-qPCR was performed using the SimpleChIP Enzymatic Chromatin IP Kit (Cell Signaling Technology). Hep3B cells were seeded in 15 cm dishes and treated with 12 μM AU-15330 or DMSO for 6 h. The cells were cross-linked with 1 % formaldehyde for 10 min, and the cross-linking was quenched using 125 mM glycine for 5 min. The cells were lysed, and the chromatin was digested with micrococcal nuclease and sheared using a Bioruptor II (Cosmo Bio, Tokyo, Japan) at high power for 10 cycles of 30 s ON

and 30 s OFF, generating DNA fragments of approximately 150–900 bp. Immunoprecipitation was performed using antibodies against c-Jun (#9165; 1:50), acetyl-histone H3 Lys27 (H3K27ac; #8173; 1:100), histone H3 (#4620; 1:50; positive control), or normal rabbit IgG (#2729; 1:500; negative control), all from Cell Signaling Technology. Enrichment at the -4.1 and -1.9 kb upstream *PLAU* enhancer regions and the +5.5 kb negative control region was quantified by qPCR using SimpleChIP Universal qPCR Master Mix (Cell Signaling Technology). The results are expressed as the percentage of input DNA. Histone H3 enrichment at ribosomal protein L30 exon 3 served as a positive ChIP control. Primer sequences were as follows: -4.1 kb, forward 5′-CCGTACCTCCTTCCCAGAACTGTTG-3′ and reverse 5′-AAGCGCCTCTTTCCCTCCTACACAT-3′; -1.9 kb, forward 5′-AAGGGGAGAAAGGGTGTCACGCTT-3′ and reverse 5′-CAGCCTGAGGACTTACCCCGAAAC-3′; and +5.5 kb, forward 5′-CCCGCTTTCTTGCTGGTTGTC-3′ and reverse 5′-CTGGTGGGTGGCACAGGCAAA-3′.

## ***PLAU* overexpression**

Hep3B and HuH-7 cells were seeded at 2 × 10^5 cells per well in 6-well plates and

transiently transfected with a *PLAU* expression plasmid, pRP[Exp]-EGFP/Neo-CMV>hPLAU, or the corresponding control plasmid, pRP[Exp]-EGFP/Neo-CMV>NC (VectorBuilder, Chicago, IL, USA), using Lipofectamine 3000 (Thermo Fisher Scientific). After 24 h, the cells were reseeded at 5,000 cells per well in 96-well plates and incubated overnight. Subsequently, the cells were treated with 0.1–100 μM AU-15330 or DMSO for 48 h, and cell viability was assessed using the CellTiter-Glo 2.0 assay. *PLAU* overexpression was confirmed by qRT-PCR, western blotting, and measurement of secreted uPA by ELISA, as described above.

**Animal study**

Six-week-old male BALB/c nude mice (Japan SLC, Shizuoka, Japan) were subcutaneously inoculated in the right flank with 2.0 × 10^7 Hep3B cells suspended in Matrigel (Corning, Corning, NY, USA). When the tumour volumes reached approximately 500 $mm^3$, mice were randomly assigned to vehicle or AU-15330 treatment groups (n = 5 per group). AU-15330 (60 mg/kg) or vehicle was administered intravenously thrice weekly for 21 days. The AU-15330 dose was selected based on a previous preclinical study (13). The vehicle consisted of 40 % polyethylene glycol 300, 5 % Tween 80, 10 % DMSO, and 45 % saline. Tumour volume and body weight were

252 measured weekly, and tumour volume was calculated as length × width² × 0.5. On day
253 21, the mice were deeply anaesthetised with isoflurane (Viatris Healthcare G.K., Tokyo,
254 Japan) and euthanised by cervical dislocation. Tumours and major organs were
255 collected for subsequent analyses. All animal procedures were approved by the Animal
256 Ethics Committee of Sapporo Medical University School of Medicine (protocol no.
257 192).

258

259 **Histological and immunohistochemical analyses**

260 Tumours and major organs were fixed in 10 % neutral-buffered formalin, paraffin-
261 embedded, and sectioned at 4 μm. The sections were stained with haematoxylin and
262 eosin for histological assessment. Tumour cell apoptosis was assessed using
263 immunohistochemical staining for cleaved PARP (#9541; Cell Signaling Technology).
264 Cleaved PARP-positive cells were counted in five randomly selected fields per tumour
265 section at ×100 magnification and averaged.

266

267 **Statistical analysis**

268 Quantitative data are presented as the mean ± standard deviation, unless otherwise

indicated. Comparisons between two groups were performed using two-tailed unpaired Student's *t*-tests or Mann–Whitney *U* tests, as appropriate. Comparisons among multiple groups were performed using one-way analysis of variance followed by Tukey's multiple-comparisons test or the Kruskal–Wallis test, as appropriate. Time- and concentration-dependent alterations in apoptosis were analysed using two-way repeated-measures analysis of variance with the Geisser–Greenhouse correction, followed by Dunnett's multiple-comparisons test comparing each time point with 0 h within each treatment group. Dose–response curves were compared using global nonlinear regression using an extra sum-of-squares *F* test. Xenograft tumour volumes at days 7, 14, and 21 were compared between the vehicle and AU-15330 groups using two-tailed unpaired Student's *t*-tests. A two-sided *P* value $< 0.05$ was considered statistically significant. Statistical analyses were performed using GraphPad Prism (version 11) and EZR (version 1.65). Statistical significance was indicated as follows: $*P < 0.05$, $** P < 0.01$, and $*** P < 0.001$.

## Results

### High *SMARCA4* expression is associated with poor overall survival in HCC

To assess the clinical relevance of SWI/SNF components in HCC, we focused on *SMARCA2* and *SMARCA4* that encode the two catalytic ATPase subunits targeted by AU-15330, and *PBRM1*, a component of the polybromo-associated BAF subclass of SWI/SNF complexes. We analysed the expression of these genes in the TCGA-LIHC cohort and compared their expression between HCC and matched adjacent non-tumour liver tissues. *SMARCA4* expression was significantly higher in HCC tissues than that in adjacent non-tumour liver tissues, whereas *SMARCA2* and *PBRM1* expression was significantly lower (Figure 1A–C). Subsequently, we assessed the associations between the expression of these genes and overall survival by comparing patients in the upper and lower quartiles of expression for each gene. Patients in the upper quartile of *SMARCA4* expression had significantly poorer overall survival than those in the lower quartile (log-rank P = 0.0169), whereas no significant differences were observed for *SMARCA2* or *PBRM1* (log-rank P = 0.1662 and 0.1125, respectively; Figure 1D–F). These findings indicate that among the SWI/SNF components examined, high *SMARCA4* expression was significantly associated with poor clinical outcomes in HCC.

## AU-15330 degrades SWI/SNF ATPase subunits and suppresses HCC cell growth

We examined the basal expression of SWI/SNF components and growth-inhibitory

304 effects of AU-15330 in three HCC cell lines. Hep3B, HuH-7, and JHH-6 cells exhibited
305 distinct expression patterns of *SMARCA2*, *SMARCA4*, and *PBRM1* and corresponding
306 proteins at the mRNA and protein levels, respectively (Figure 2A, B). Treatment with 1
307 μM AU-15330 for 24 h significantly reduced SMARCA2 and SMARCA4 protein levels
308 in all three cell lines and was accompanied by a reduction in PBRM1 protein levels
309 (Figure 2C). AU-15330 reduced cell viability in a concentration-dependent manner,
310 although sensitivity differed among the three cell lines (Figure 2D). Hep3B cells were
311 the most sensitive ($IC_{50}$ of 8.9 μM), followed by HuH-7 cells ($IC_{50}$ of 21.1 μM), whereas
312 an $IC_{50}$ could not be determined for JHH-6 cells at concentrations up to 100 μM.
313 Notably, AU-15330 sensitivity ranked consistently with basal SMARCA4 protein
314 expression across the three cell lines (Figure 2B), indicating a potential association
315 between SMARCA4 abundance and AU-15330 sensitivity. Therefore, Hep3B cells,
316 which exhibited the highest sensitivity to AU-15330, were used for most subsequent
317 experiments, with selected findings independently evaluated in HuH-7 cells.

318

319 **AU-15330 induces apoptosis in a time- and dose-dependent manner**

320 To determine whether AU-15330-mediated growth inhibition was associated with
321 apoptotic cell death, we examined apoptosis in Hep3B cells. Flow cytometric analysis

after 48 h of treatment demonstrated a dose-dependent increase in the total apoptotic cells, defined as the combined Annexin $V^+/7\text{-}AAD^-$ and Annexin $V^+/7\text{-}AAD^+$ populations (Figure 2E, F). The proportion of total apoptotic cells increased from 5.7 % in vehicle-treated cells to 72.8 and 92.7 % after treatment with 12 and 18 μM AU-15330, respectively. Subsequently, we monitored apoptosis over 24 h using a luminescence-based Annexin V assay. Annexin V-derived luminescence increased over time in an AU-15330 concentration-dependent manner, with a time-by-concentration interaction (Figure S1A, B). The apoptotic signal became evident 12 h after AU-15330 exposure and increased thereafter. Western blotting detected cleaved PARP from 24 h, accompanied by a progressive reduction in full-length PARP protein (Figure 2G). These results demonstrated that AU-15330 induces apoptotic cell death in Hep3B cells in a dose- and time-dependent manner.

## AU-15330 inhibits HCC xenograft growth in vivo

We assessed the antitumour activity of AU-15330 in vivo using a Hep3B xenograft model in BALB/c nude mice (Figure 3A). Tumours continued to grow in vehicle-treated mice, whereas tumour growth was significantly suppressed by AU-15330 treatment (Figure 3B, C). The difference became significant on day 21, when the mean tumour

volume was 4492 ± 1456 and 1452 ± 959 $mm^3$ in the vehicle and AU-15330 groups, respectively ($P = 0.0079$), corresponding to an approximately 68 % reduction in tumour volume. Histological analysis of xenograft tumours exhibited increased cleaved PARP positivity following AU-15330 treatment, consistent with enhanced apoptosis in vivo (Figure 3D, E). AU-15330 treatment did not significantly affect body weight during the treatment period (Figure S2A), and no apparent histopathological abnormalities were observed in the liver, lung, heart, or kidney (Figure S2B). Together, these findings demonstrated that AU-15330 suppresses HCC xenograft growth in vivo without overt systemic toxicity.

## AU-15330 induces rapid and sustained suppression of *PLAU* expression

To identify the downstream transcriptional programs associated with the antitumour activity of AU-15330, we performed RNA sequencing of Hep3B cells treated with AU-15330 or vehicle. Because AU-15330-induced apoptotic signals became apparent from 12 h onwards, cells were analysed at 6 and 12 h to capture transcriptional alterations preceding and accompanying apoptosis onset (Figure 4A). Thirty differentially expressed genes were identified at 6 h and 157 at 12 h using an adjusted $P$ value < 0.01 and absolute $\log_2$ fold change > 2 as the significance thresholds (Figure 4B). Of these,

22 differentially expressed genes were common to both time points, 21 of which were downregulated by AU-15330 at 6 h (Figure 4C). Pentraxin 3 exhibited the largest reduction at 6 h, with $\log_2$ fold changes of -3.125 and -3.022 at 6 and 12 h, respectively. In contrast, *PLAU* exhibited the second-largest reduction at 6 h and was further suppressed at 12 h, with $\log_2$ fold changes of -2.846 and -3.359, respectively. Based on this rapid and sustained transcriptional suppression, *PLAU* was selected as a candidate downstream effector of AU-15330 for further assessment.

We examined the early effects of AU-15330 on the *PLAU*/uPA axis. qRT-PCR revealed that *PLAU* mRNA expression was significantly reduced as early as 3 h after AU-15330 treatment, and this suppression was maintained for 12 h (Figure 5A). Consistent with the reduction in *PLAU* transcript levels, the concentration of secreted uPA in culture supernatants was significantly reduced following AU-15330 treatment (Figure 5B). We further examined the *PLAU*/uPA axis in Hep3B xenograft tumours. *PLAU* mRNA expression was significantly lower in tumours from AU-15330-treated mice than in those from vehicle-treated mice (Figure 5C). Additionally, uPA protein expression was reduced in AU-15330-treated xenograft tumours (Figure 5D). Together, these findings indicated that AU-15330 suppresses the *PLAU*/uPA axis in vitro and in vivo.

## AU-15330 reduces c-Jun occupancy and H3K27ac enrichment at *PLAU* enhancer regions

Because AU-15330 degrades SWI/SNF ATPases, we subsequently assessed whether the suppression of *PLAU* transcription was associated with altered enhancer regulation. Previous studies have implicated the activator protein-1 complex, specifically c-Jun, in the transcriptional regulation of PLAU through upstream enhancer regions (16, 17). Therefore, we performed ChIP-qPCR for c-Jun and H3K27ac at two upstream *PLAU* enhancer regions located approximately 4.1 (P1; enhancer 1) and 1.9 kb (P2; enhancer 2) from the transcription start site, using the +5.5-kb region (P3) as a negative control (Figure 6A). The technical validity of the ChIP assay was supported by robust histone H3 enrichment at the ribosomal protein L30 exon 3 positive-control region and minimal IgG enrichment at the ribosomal protein L30 exon 3 and examined *PLAU* regions (Figure S3A, B).

AU-15330 treatment significantly reduced c-Jun occupancy at both P1 and P2, whereas no significant alterations were observed at the P3 negative-control region (Figure 6B). Similarly, H3K27ac enrichment was significantly reduced at P1 and P2, with no significant alterations at P3 (Figure 6C). To determine whether the reduction in

c-Jun occupancy was associated with alterations in c-Jun abundance or activation, we examined total c-Jun and phospho-c-Jun (Ser73) protein levels. AU-15330 did not significantly alter total c-Jun or phospho-c-Jun (Ser73) levels during the 12-hour treatment period (Figure 6D). Together, these findings indicated that AU-15330 reduces c-Jun occupancy and H3K27ac enrichment at upstream *PLAU* enhancer regions without significantly altering c-Jun abundance or Ser73 phosphorylation.

## PLAU overexpression partially attenuates AU-15330-induced growth inhibition

To determine whether *PLAU* suppression contributes functionally to the growth-inhibitory effects of AU-15330, we transiently overexpressed *PLAU* in Hep3B cells. *PLAU* overexpression was confirmed at the mRNA and protein levels by qRT-PCR and western blotting, respectively, and was accompanied by increased uPA secretion into the culture supernatant (Figure 7A–C). Subsequently, we compared the effects of AU-15330 on cell viability in *PLAU*-overexpressing and control cells. *PLAU* overexpression shifted the AU-15330 dose–response curve to the right, increasing the $IC_{50}$ from 12.1 μM in control cells to 19.5 μM in *PLAU*-overexpressing cells (Figure 7D). The dose–response curves differed significantly based on global nonlinear regression with an extra sum-of-squares *F* test ($P < 0.0001$). To assess whether these effects were reproducible in

another HCC cell line, we performed similar experiments using HuH-7 cells. AU-15330 induced apoptosis in a concentration-dependent manner and reduced *PLAU* expression and uPA secretion in HuH-7 cells (Figure S4A–E). Moreover, *PLAU* overexpression shifted the AU-15330 dose–response curve to the right, increasing the $IC_{50}$ from 15.8 μM in control cells to 22.0 μM in *PLAU*-overexpressing cells (Figure S5A–D). These findings were consistent with those obtained in Hep3B cells. Together, these results support a functional contribution of *PLAU* suppression to the antitumour effects of AU-15330 across multiple HCC cell models.

## Discussion

In this study, the pharmacologic degradation of SWI/SNF ATPases by AU-15330 suppressed HCC growth in vitro and in vivo and induced apoptosis cell death. In the TCGA-LIHC cohort, patients in the upper quartile of *SMARCA4* expression had poorer overall survival than those in the lower quartile. Basal SMARCA4 protein abundance across the three HCC cell lines paralleled their sensitivity to AU-15330. Mechanistically, AU-15330 rapidly suppressed *PLAU* transcription and reduced c-Jun occupancy and H3K27ac enrichment at the upstream *PLAU* enhancer regions without significantly altering c-Jun abundance or Ser73 phosphorylation. Additionally, *PLAU*

overexpression partially attenuated AU-15330-induced growth inhibition. Selected findings, including AU-15330-induced apoptosis, suppression of the *PLAU*/uPA axis, and attenuation of AU-15330 sensitivity by *PLAU* overexpression, were also observed in HuH-7 cells. Together, these findings identify *PLAU* repression as a functionally relevant downstream component of the antitumour activity of SWI/SNF ATPase degradation in HCC.

The antitumour activity of AU-15330 observed in this study indicates that SWI/SNF ATPase activity may contribute to the maintenance of HCC cell survival. *SMARCA4*—that encodes the Brahma-related gene 1 catalytic ATPase subunit of the SWI/SNF complex—is recurrently altered across multiple human cancer types (12). In the TCGA-LIHC cohort, patients in the upper quartile of *SMARCA4* expression had poorer overall survival than those in the lower quartile. This association indicates that high *SMARCA4* expression may characterise a clinically unfavourable subset of HCC. Additionally, AU-15330 sensitivity rankings across the three HCC cell lines paralleled their basal SMARCA4 protein abundance. Although this observation indicates that SMARCA4 abundance may be associated with sensitivity to SWI/SNF ATPase degradation, the limited number of cell lines precludes conclusions regarding its predictive value. Consistent with the antitumour activity previously reported for AU-15330 in enhancer-

dependent prostate cancer models (13), AU-15330 induced apoptosis and suppressed xenograft growth in the present HCC models. These findings indicate that SWI/SNF ATPase dependency may extend to a subset of HCCs and highlight the need to define molecular determinants of sensitivity to AU-15330.

A central mechanistic finding of this study is that SWI/SNF ATPase degradation suppresses *PLAU* transcription in association with altered enhancer regulation. *PLAU* encodes uPA that facilitates extracellular matrix degradation, invasion, angiogenesis, and metastatic progression through the plasminogen–plasmin system (18). In HCC, increased activity of the uPA system has been associated with invasive behaviour and poor clinical outcomes (19, 20). In this study, AU-15330 reduced c-Jun occupancy and H3K27ac enrichment at upstream *PLAU* enhancer regions without significantly altering total c-Jun or phospho-c-Jun (Ser73) protein levels. This pattern indicates that *PLAU* repression is associated with alterations in enhancer activity or accessibility rather than with reduced c-Jun abundance or activation. Notably, *PLAU* overexpression partially attenuated AU-15330-induced growth inhibition, supporting a functional contribution of *PLAU* suppression to the antitumour effect. Taken together, these findings indicate that SWI/SNF ATPase activity maintains *PLAU* transcription through enhancer-associated regulation, and AU-15330 disrupts this regulatory state in HCC cells.

These findings indicate that dependence on SWI/SNF ATPase activity may characterise a biologically distinct subset of HCC. SWI/SNF complexes regulate broad transcriptional programs; therefore, their degradation is unlikely to exert antitumour effects through a single downstream target. In this study, the *PLAU*/uPA axis suppression emerged as a functionally relevant consequence of AU-15330 treatment. However, PLAU overexpression only partially attenuated AU-15330-induced growth inhibition. This finding indicates that additional transcriptional programs likely contribute to the antitumour effects of SWI/SNF ATPase degradation. Identifying these downstream pathways will help clarify the molecular basis of AU-15330 sensitivity in HCC. Moreover, it will be crucial to determine whether SMARCA4 expression or other SWI/SNF dependency-associated molecular features can identify tumours that are more sensitive to AU-15330. These studies may help define the HCC subgroups in which SWI/SNF ATPase degradation is most likely to have a therapeutic value.

This study has several limitations. First, the association between SMARCA4 protein abundance and AU-15330 sensitivity was assessed in only three HCC cell lines. Therefore, studies using a broader panel of HCC models are required to determine whether SMARCA4 expression or other molecular features can predict sensitivity to SWI/SNF ATPase degradation. Second, RNA sequencing was performed using two

biological replicates per condition and was used primarily to identify candidate downstream genes. Although *PLAU* suppression was subsequently validated by independent approaches, transcriptome-wide alterations induced by AU-15330 will require confirmation in larger datasets. Third, this study did not examine genome-wide alterations in chromatin accessibility or transcription factor occupancy. ATAC-seq and genome-wide ChIP-based analyses can clarify how SWI/SNF ATPase degradation alters enhancer activity and determine whether the alterations observed at the *PLAU* locus reflect a broader transcriptional response. Finally, the in vivo experiments were performed using a subcutaneous Hep3B xenograft model in immunodeficient mice. Additional studies using orthotopic and immunocompetent models are needed to assess the effects of SWI/SNF ATPase degradation within the hepatic tumour microenvironment and assess its potential interactions with antitumour immunity.

Despite these limitations, our findings demonstrate that AU-15330 suppresses HCC growth in vitro and in vivo and PLAU repression partially contributes to this antitumour effect. The accompanying reduction in c-Jun occupancy and H3K27ac enrichment at upstream PLAU enhancer regions further supports an association between SWI/SNF ATPase degradation and altered enhancer-associated transcription. Further studies are

warranted to define the broader transcriptional consequences of SWI/SNF ATPase degradation and identify HCC subsets most likely to benefit from this approach.

## References


1. Bray F, Laversanne M, Sung H, Ferlay J, Siegel RL, Soerjomataram I, et al. Global cancer statistics 2022: GLOBOCAN estimates of incidence and mortality worldwide for 36 cancers in 185 countries. CA Cancer J Clin. 2024;74(3):229-63.
2. Gujarathi R, Klein JA, Liao CY, Pillai A. The Changing Demographics and Epidemiology of Hepatocellular Carcinoma. Clin Liver Dis. 2025;29(1):1-15.
3. Llovet JM, Ricci S, Mazzaferro V, Hilgard P, Gane E, Blanc JF, et al. Sorafenib in advanced hepatocellular carcinoma. N Engl J Med. 2008;359(4):378-90.
4. Kudo M, Finn RS, Qin S, Han KH, Ikeda K, Piscaglia F, et al. Lenvatinib versus sorafenib in first-line treatment of patients with unresectable hepatocellular carcinoma: a randomised phase 3 non-inferiority trial. Lancet. 2018;391(10126):1163-73.
5. Finn RS, Qin S, Ikeda M, Galle PR, Ducreux M, Kim TY, et al. Atezolizumab plus Bevacizumab in Unresectable Hepatocellular Carcinoma. N Engl J Med. 2020;382(20):1894-905.
6. Abou-Alfa GK, Lau G, Kudo M, Chan SL, Kelley RK, Furuse J, et al. Tremelimumab plus Durvalumab in Unresectable Hepatocellular Carcinoma. NEJM Evid. 2022;1(8):EVIDoa2100070.
7. Yau T, Galle PR, Decaens T, Sangro B, Qin S, da Fonseca LG, et al. Nivolumab plus ipilimumab versus lenvatinib or sorafenib as first-line treatment for unresectable hepatocellular carcinoma (CheckMate 9DW): an open-label, randomised, phase 3 trial. Lancet. 2025;405(10492):1851-64.
8. Jones PA, Baylin SB. The fundamental role of epigenetic events in cancer. Nat Rev Genet. 2002;3(6):415-28.
9. Esteller M. Epigenetics in cancer. N Engl J Med. 2008;358(11):1148-59.
10. Kadoch C, Hargreaves DC, Hodges C, Elias L, Ho L, Ranish J, et al. Proteomic and bioinformatic analysis of mammalian SWI/SNF complexes identifies extensive roles in human malignancy. Nat Genet. 2013;45(6):592-601.
11. Shain AH, Pollack JR. The spectrum of SWI/SNF mutations, ubiquitous in human cancers. PLoS One. 2013;8(1):e55119.
12. Peng L, Li J, Wu J, Xu B, Wang Z, Giamas G, et al. A Pan-Cancer Analysis of SMARCA4 Alterations in Human Cancers. Front Immunol. 2021;12:762598.
13. Xiao L, Parolia A, Qiao Y, Bawa P, Eyunni S, Mannan R, et al. Targeting SWI/SNF ATPases in enhancer-addicted prostate cancer. Nature. 2022;601(7893):434-9.
14. Kanda Y. Investigation of the freely available easy-to-use software 'EZR' for medical statistics. Bone Marrow Transplant. 2013;48(3):452-8.
15. Heberle H, Meirelles GV, da Silva FR, Telles GP, Minghim R. InteractiVenn: a

web-based tool for the analysis of sets through Venn diagrams. BMC Bioinformatics. 2015;16(1):169.
16. Tullai JW, Tacheva S, Owens LJ, Graham JR, Cooper GM. AP-1 is a component of the transcriptional network regulated by GSK-3 in quiescent cells. PLoS One. 2011;6(5):e20150.
17. Ferrai C, Munari D, Luraghi P, Pecciarini L, Cangi MG, Doglioni C, et al. A transcription-dependent micrococcal nuclease-resistant fragment of the urokinase-type plasminogen activator promoter interacts with the enhancer. J Biol Chem. 2007;282(17):12537-46.
18. Mahmood N, Mihalcioiu C, Rabbani SA. Multifaceted Role of the Urokinase-Type Plasminogen Activator (uPA) and Its Receptor (uPAR): Diagnostic, Prognostic, and Therapeutic Applications. Front Oncol. 2018;8:24.
19. Zheng Q, Tang ZY, Xue Q, Shi DR, Song HY, Tang HB. Invasion and metastasis of hepatocellular carcinoma in relation to urokinase-type plasminogen activator, its receptor and inhibitor. J Cancer Res Clin Oncol. 2000;126(11):641-6.
20. Tsai MC, Yen YH, Chang KC, Hung CH, Chen CH, Lin MT, et al. Elevated levels of serum urokinase plasminogen activator predict poor prognosis in hepatocellular carcinoma after resection. BMC Cancer. 2019;19(1):1169.

## Data Availability Statement

The datasets used and/or analysed during the current study are available from the corresponding author upon reasonable request. The RNA sequencing data have been submitted to the DNA Data Bank of Japan Sequenced Read Archive under the accession numbers DRR1093361-DRR1093370.

## Acknowledgements

We would like to thank Editage (www.editage.jp) for English language editing.

## Author contributions

K. Takada and Y. Kawano contributed to the study concept. Y. Kawano contributed to the experimental designs. N. Suzuki, T. Kubo, Y. Arihara, T. Kubo, Y. Okagawa, M. Hirakawa, R. Yokoyama, H. Watabe, and S. Kubota and contributed to data generation. R. Maruyama and K. Takada contributed to data analysis. K. Takada, N. Suzuki, and Y. Kawano drafted the manuscript. All authors provided crucially reviewed the manuscript.

## Competing Interests

K.T. received lecture fees from Daiichi Sankyo, Chugai Pharmaceutical, Eisai, Ono Pharmaceutical, Eli Lilly, Sanofi, Takeda Pharmaceutical, Sysmex, Janssen Pharmaceutical, Otsuka Pharmaceutical, MSD, EA Pharma, Zeria Pharmaceutical,

Kyowa Kirin Co., and Gilead Sciences. K.T. received research funding from AbbVie and Taiho. The other authors declare no competing interests.

## Funding Information

This work was supported by JSPS KAKENHI Grant Number 22K08080.

## Figure Legends

**Figure. 1. Expression and prognostic significance of SWItch/sucrose non-fermentable components in hepatocellular carcinoma.**

(A–C) Expression of SWI/SNF-related, matrix-associated, actin-dependent regulator of chromatin, subfamily A (*SMARCA*)2 (A), *SMARCA4* (B), and polybromo-1 (*PBRM1*) (C) in hepatocellular carcinoma and adjacent non-tumour liver tissues in The Cancer Genome Atlas Liver Hepatocellular Carcinoma cohort (n = 50 paired samples). Differences between paired tumour and adjacent non-tumour liver tissues are assessed using the Wilcoxon signed-rank test. (D–F) Kaplan–Meier analysis of overall survival according to *SMARCA2* (D), *SMARCA4* (E), and *PBRM1* (F) expression. Patients in the upper quartile (75th–100th percentile) and lower quartile (0–25th percentile) of expression for each gene are compared. Survival differences are assessed using the log-rank test. *$P < 0.05$ and ***$P < 0.001$; n.s., not significant.

**Figure 2. AU-15330 degrades SWItch/sucrose non-fermentable ATPase subunits and suppresses hepatocellular carcinoma cell growth.**

(A) Relative mRNA expression of SWI/SNF-related, matrix-associated, actin-dependent

596 regulator of chromatin, subfamily A (*SMARCA*)*4*, *SMARCA2*, and polybromo-1
597 (*PBRM1*) in Hep3B, HuH-7, and JHH-6 cells. (B) Basal protein expression of
598 SMARCA4, SMARCA2, and PBRM1 in the three hepatocellular carcinoma cell lines.
599 (C) Western blot analysis of SMARCA4, SMARCA2, and PBRM1 after treatment with
600 1 μM AU-15330 for 24 h. β-Actin is used as a loading control. Numbers below the blots
601 indicate relative protein expression normalised to β-actin. The samples derive from the
602 same experiment but different gels were processed in parallel. (D) Cell viability of JHH-
603 6, HuH-7, and Hep3B cells after treatment with increasing concentrations of AU-15330
604 for 48 h. Half-maximal inhibitory concentration values are 8.9 μM for Hep3B and 21.1
605 μM for HuH-7 cells; the half-maximal inhibitory concentration is not reached in JHH-6
606 cells within the tested concentration range of up to 100 μM. Data are presented as the
607 mean ± standard deviation (n = 3). (E) Representative flow cytometry plots of Hep3B
608 cells treated with vehicle or 6, 12, or 18 μM AU-15330 for 48 h and stained with
609 phycoerythrin-conjugated Annexin V and 7-AAD. Early apoptotic cells are defined as
610 Annexin $V^+$/7-$AAD^-$, and late apoptotic cells are defined as Annexin $V^+$/7-$AAD^+$. (F)
611 Quantification of total apoptotic cells, defined as the sum of early and late apoptotic
612 populations. (G) Western blot analysis of poly (ADP-ribose) polymerase (PARP) and
613 cleaved PARP in Hep3B cells treated with 12 μM AU-15330 or dimethyl sulfoxide

(DMSO) for 0, 24, or 48 h. β-Actin is used as a loading control. Data in (F) are presented as the mean ± standard deviation (n = 3). *$P < 0.05$ and ***$P < 0.001$.

**Figure 3. AU-15330 inhibits hepatocellular carcinoma xenograft growth in vivo.** (A) Experimental design of the Hep3B xenograft study. Mice bearing subcutaneous Hep3B tumours are randomly assigned to vehicle or AU-15330 treatment groups when tumour volumes reached approximately 500 $mm^3$. AU-15330 is administered intravenously at 60 mg/kg thrice weekly for 21 days (n = 5 per group). (B) Tumour growth curves during the treatment period. Tumour volumes are compared between groups at the indicated time points using two-tailed unpaired Student's t-tests. (C) Representative images of tumour-bearing mice on days 0, 7, and 21 after treatment initiation. (D) Representative haematoxylin and eosin-stained and cleaved poly (ADP-ribose) polymerase-immunostained sections of xenograft tumours from vehicle- and AU-15330-treated mice. Scale bars, 100 μm. (E) Quantification of cleaved PARP cells per high-power field (HPF). Five randomly selected fields are assessed for each tumour section at ×100 magnification. Data are presented as the mean ± standard deviation. **$P < 0.01$; n.s., not significant.

**Figure 4. RNA sequencing identifies *plasminogen activator, urokinase (PLAU)* as a candidate downstream effector of AU-15330.**

(A) Experimental design for RNA sequencing of Hep3B cells treated with 12 μM AU-15330 or dimethyl sulfoxide (DMSO) for 6 or 12 h. RNA sequencing is performed with two biological replicates per condition. Differentially expressed genes (DEGs) are defined as genes with an adjusted $P < 0.01$ and absolute $\log_2$ fold change > 2. (B) Venn diagram demonstrating DEGs identified at 6 and 12 h and their overlap. Thirty DEGs are identified at 6 h and 157 at 12 h, with 22 DEGs common to both time points. (C) Heatmap demonstrating $\log_2$ fold changes of the 22 DEGs common to both time points.

**Figure 5. AU-15330 suppresses the plasminogen activator, urokinase/urokinase-type plasminogen activator axis, both in vitro and in vivo.**

(A) Relative expression of *plasminogen activator, urokinase (PLAU)* mRNA in Hep3B cells treated with 12 μM AU-15330 or dimethyl sulfoxide (DMSO)for 3, 6, or 12 h, as determined by quantitative reverse transcription-polymerase chain reaction. Expression levels are normalised to those of the corresponding DMSO-treated controls. Data are presented as the mean ± standard deviation (SD) (n = 3). (B) Urokinase-type plasminogen activator (uPA) concentrations in culture supernatants from Hep3B cells

650 treated with 12 μM AU-15330 or DMSO for the indicated times, as determined by
651 ELISA. Data are presented as the mean ± SD (n = 3). Control refers to the sample taken
652 at the start of treatment. (C) Relative expression of *PLAU* mRNA in Hep3B xenograft
653 tumours from vehicle- and AU-15330-treated mice. Data are presented as the mean ±
654 SD (n = 5 per group). (D) Western blot analysis of uPA protein expression in Hep3B
655 xenograft tumours from vehicle- and AU-15330-treated mice (n = 5 tumours per group).
656 β-Actin was used as a loading control. The samples derive from the same experiment
657 but different gels were processed in parallel. Data are presented as the mean ± SD. *$P <$
658 0.05 and ***$P < 0.001$.
659
660 **Figure 6. AU-15330 reduces c-Jun occupancy and H3K27ac enrichment at**
661 ***plasminogen activator, urokinase* (*PLAU*) enhancer regions.**
662 A) Schematic representation of the *plasminogen activator, urokinase* (*PLAU*) locus
663 demonstrating the -4.1-kb (P1; enhancer 1) and -1.9-kb (P2; enhancer 2) regions
664 upstream of the transcription start site and the +5.5-kb region (P3) used as a negative
665 control for ChIP-qPCR. (B) c-Jun occupancy at P1, P2, and P3 in Hep3B cells treated
666 with 12 μM AU-15330 or dimethyl sulfoxide (DMSO) for 6 h. ChIP enrichment is
667 expressed as the percentage of input DNA. Data are presented as the mean ± standard

deviation (n = 3). (C) H3K27ac enrichment at P1, P2, and P3 in Hep3B cells treated with 12 μM AU-15330 or DMSO for 6 h. ChIP enrichment is expressed as percentage of input DNA. Data are presented as the mean ± standard deviation (n = 3). (D) Western blot analysis of total c-Jun and phospho-c-Jun (Ser73) in Hep3B cells treated with 12 μM AU-15330 or DMSO for 0, 3, 6, or 12 h. β-Actin is used as a loading control. The samples derive from the same experiment but different gels were processed in parallel. $^{**}P < 0.01$ and $^{***}P < 0.001$; n.s., not significant.

**Figure 7. *Plasminogen activator, urokinase (PLAU)* overexpression partially attenuates AU-15330-induced growth inhibition in Hep3B cells.**

(A) Western blot analysis of urokinase-type plasminogen activator (uPA) and green fluorescent protein in Hep3B cells transfected with a *PLAU* expression vector (PLAU OE), control vector, or mock control. β-Actin is used as a loading control. (B) Relative *PLAU* mRNA expression in PLAU-overexpressing, control vector-transfected, and mock-transfected Hep3B cells. Data are presented as the mean ± standard deviation (n = 3). (C) Urokinase-type plasminogen activator (uPA) concentrations in culture supernatants from *PLAU*-overexpressing, control vector-transfected, and mock-transfected Hep3B cells, as determined by enzyme-linked immunosorbent assay. Data

are presented as the mean ± standard deviation (n = 3). (D) Dose–response curves of *PLAU*-overexpressing and control vector-transfected Hep3B cells after treatment with AU-15330 for 48 h. The half-maximal inhibitory concentration values are 19.5 and 12.1 μM in *PLAU*-overexpressing and control cells, respectively. Dose–response curves are compared using global nonlinear regression with an extra sum-of-squares *F* test (***$P$ < 0.001). Data are presented as the mean ± standard deviation (n = 3). ***$P$ < 0.001; n.s., not significant.

**Figure S1. Time-course analysis of AU-15330-induced apoptosis in Hep3B cells.** (A) Annexin V-associated luminescence in Hep3B cells treated with 6, 12, or 18 μM AU-15330 or 1 μM staurosporine and monitored for 24 h using the RealTime-Glo™ Annexin V Apoptosis Assay. Luminescence values are corrected by subtracting the corresponding vehicle-treated value at each time point. (B) Time-course profiles of Annexin V-associated luminescence for each treatment condition. Data are presented as the mean ± standard deviation (n = 4). Time-dependent alterations are analysed using two-way repeated-measures analysis of variance with the Geisser–Greenhouse correction, followed by Dunnett's multiple-comparisons test comparing each time point with 0 h within each treatment group. *$P$ < 0.05, **$P$ < 0.01, and ***$P$ < 0.001.

**Figure S2. Assessment of body weight and histopathological alterations during AU-15330 treatment.**

(A) Relative body weight of mice bearing Hep3B xenografts during treatment with vehicle or AU-15330. Body weight was normalised to the value at treatment initiation (day 0 = 1.0). Data are presented as the mean ± standard deviation (n = 5 per group). Differences between groups at the indicated time points are analysed using two-tailed unpaired Student's t-tests; n.s., not significant. (B) Representative haematoxylin and eosin-stained sections of the liver, lung, heart, and kidney collected at the end of the 21-day treatment period. Scale bars, 100 μm. n.s., not significant.

**Figure S3. Technical validation of the chromatin immunoprecipitation–quantitative polymerase chain reaction assay.**

(A) Histone H3 enrichment at the ribosomal protein L30 exon 3 positive-control region in Hep3B cells treated with 12 μM AU-15330 or dimethyl sulfoxide (DMSO) for 6 h. Chromatin immunoprecipitation enrichment is expressed as the percentage of input DNA. (B) Normal rabbit IgG enrichment at the ribosomal protein L30 exon 3 region and examined plasminogen activator, urokinase (PLAU) regions in Hep3B cells treated

722 with 12 μM AU-15330 or DMSO for 6 h. Chromatin immunoprecipitation enrichment is
723 expressed as the percentage of input DNA. Data are presented as the mean ± standard
724 deviation (n = 3).
725
726 **Figure S4. AU-15330 induces apoptosis and suppresses the *PLAU*/uPA axis in HuH-**
727 **7 cells.**
728 (A) Representative flow cytometry plots of HuH-7 cells treated with vehicle or 12, 24,
729 or 36 μM AU-15330 for 48 h and stained with phycoerythrin-conjugated Annexin V and
730 7-AAD. Early apoptotic cells are defined as Annexin $V^+$/7-$AAD^-$, and late apoptotic
731 cells are defined as Annexin $V^+$/7-$AAD^+$. (B) Quantification of total apoptotic cells,
732 defined as the sum of early and late apoptotic populations. (C) Western blot analysis of
733 poly (ADP-ribose) polymerase and cleaved PARP in HuH7 cells treated with 24 μM
734 AU-15330 or dimethyl sulfoxide (DMSO) for 0, 24, or 48 h. β-Actin is used as a
735 loading control. Data in (B) are presented as the mean ± standard deviation (n = 3). (D)
736 Relative expression of *plasminogen activator, urokinase (PLAU)* mRNA in HuH-7 cells
737 treated with 24 μM AU-15330 or DMSO for 3, 6, or 12 h, as determined by quantitative
738 reverse transcription-polymerase chain reaction. Expression levels are normalised to
739 those of the corresponding DMSO-treated controls. Data are presented as the mean ±

740 standard deviation (SD) (n = 3). (E) Urokinase-type plasminogen activator (uPA)
741 concentrations in culture supernatants from HuH-7 cells treated with 24 μM AU-15330
742 or DMSO for the indicated times, as determined by ELISA. Data are presented as the
743 mean ± SD (n = 3). Control refers to the sample taken at the start of treatment. ***$P <$
744 0.001.

745

746 **Figure S5. *PLAU* overexpression partially attenuates AU-15330-induced growth**
747 **inhibition in HuH-7 cells.**
748 (A) Western blot analysis of urokinase-type plasminogen activator (uPA) and green
749 fluorescent protein in HuH-7 cells transfected with a *PLAU* expression vector (PLAU
750 OE), control vector, or mock control. β-Actin is used as a loading control. (B) Relative
751 *PLAU* mRNA expression in *PLAU*-overexpressing, control vector-transfected, and
752 mock-transfected HuH-7 cells. Data are presented as the mean ± standard deviation (n =
753 3). (C) Urokinase-type plasminogen activator (uPA) concentrations in culture
754 supernatants from *PLAU*-overexpressing, control vector-transfected, and mock-
755 transfected HuH-7 cells, as determined by enzyme-linked immunosorbent assay. Data
756 are presented as the mean ± standard deviation (n = 3). (D) Dose–response curves of
757 *PLAU*-overexpressing and control vector-transfected HuH-7 cells after treatment with

AU-15330 for 48 h. The half-maximal inhibitory concentration values are 22.0 and 15.8 μM in *PLAU*-overexpressing and control cells, respectively. Dose–response curves are compared using global nonlinear regression with an extra sum-of-squares F test (***$P$ < 0.001). Data are presented as the mean ± standard deviation (n = 3). ***$P$ < 0.001; n.s., not significant.

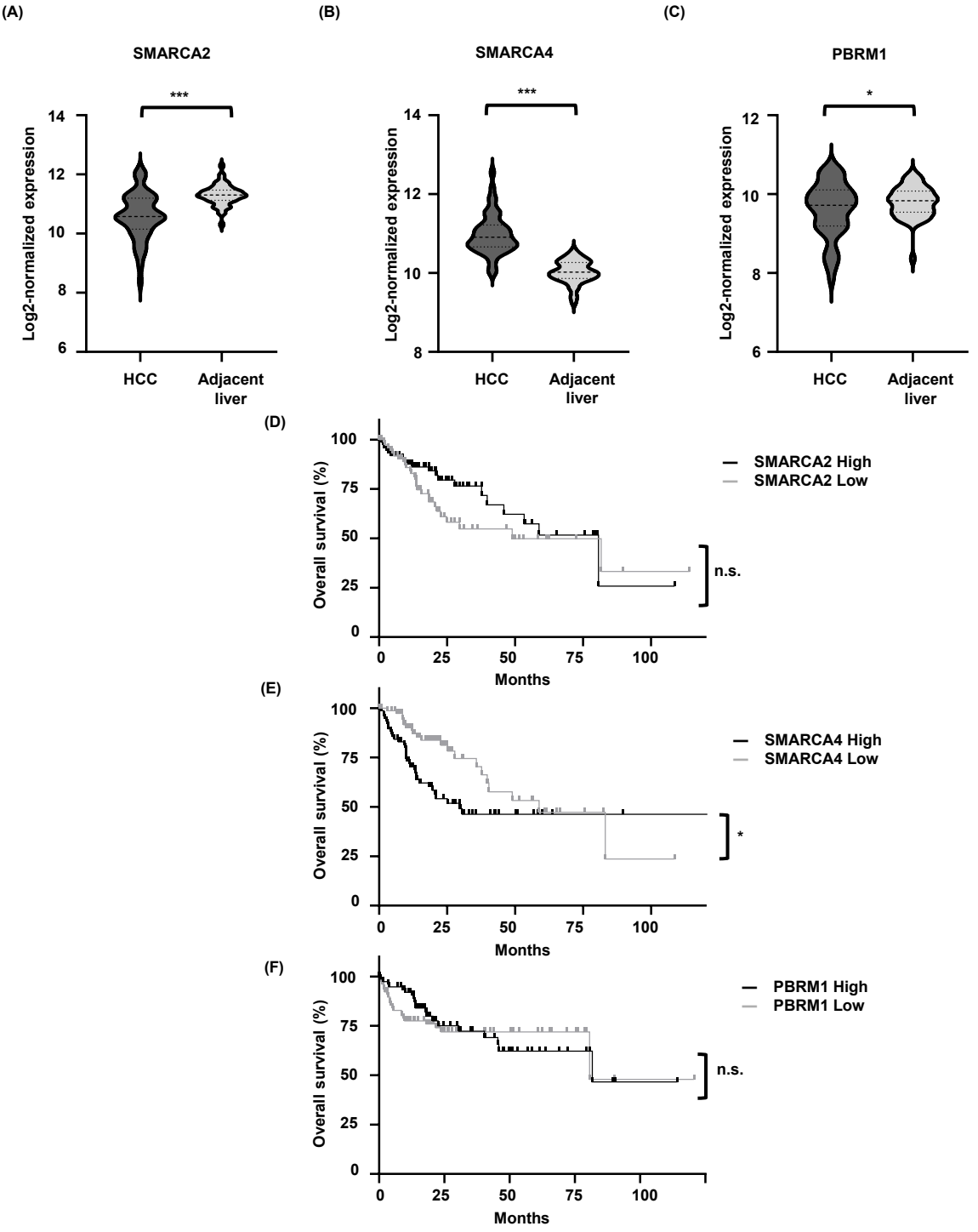
(A)
SMARCA2
***
Log2-normalized expression
14
12
10
8
6
HCC
Adjacent liver
(B)
SMARCA4
***
Log2-normalized expression
14
12
10
8
HCC
Adjacent liver
(C)
PBRM1
*
Log2-normalized expression
12
10
8
6
HCC
Adjacent liver
(D)
Overall survival (%)
100
75
50
25
0
0
25
50
75
100
Months
SMARCA2 High
SMARCA2 Low
n.s.
(E)
Overall survival (%)
Months
SMARCA4 High
SMARCA4 Low
*
(F)
Overall survival (%)
Months
PBRM1 High
PBRM1 Low
n.s.

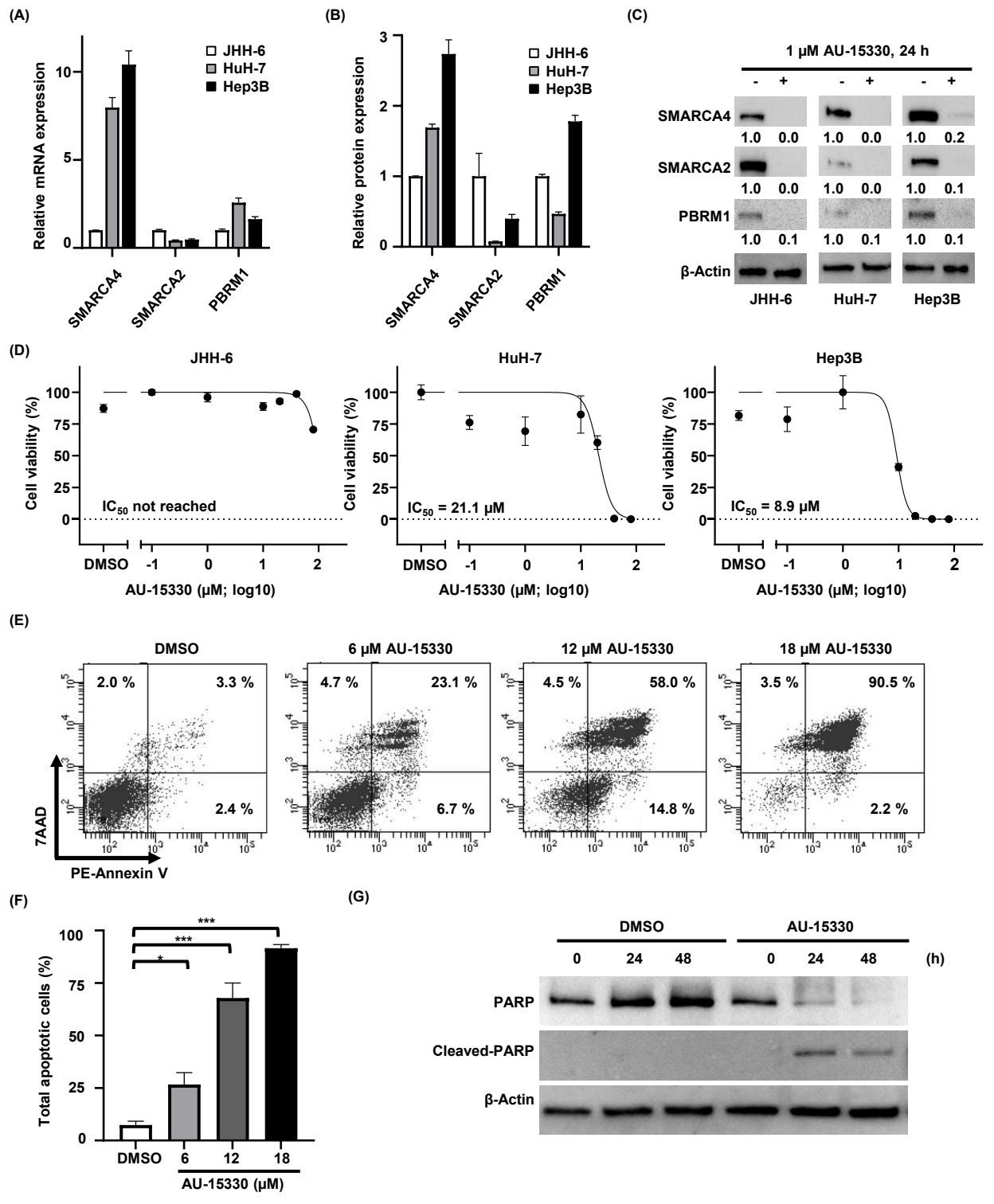
(A)
Relative mRNA expression
JHH-6
HuH-7
Hep3B
SMARCA4
SMARCA2
PBRM1
(B)
Relative protein expression
(C)
1 μM AU-15330, 24 h
SMARCA4
SMARCA2
PBRM1
β-Actin
1.0 0.0 1.0 0.0 1.0 0.2
1.0 0.0 1.0 0.0 1.0 0.1
1.0 0.1 1.0 0.1 1.0 0.1
(D)
Cell viability (%)
IC50 not reached
IC50 = 21.1 μM
IC50 = 8.9 μM
DMSO
AU-15330 (μM; log10)
(E)
DMSO
6 μM AU-15330
12 μM AU-15330
18 μM AU-15330
2.0 % 3.3 % 2.4 %
4.7 % 23.1 % 6.7 %
4.5 % 58.0 % 14.8 %
3.5 % 90.5 % 2.2 %
7AAD
PE-Annexin V
(F)
Total apoptotic cells (%)
DMSO
AU-15330 (μM)
(G)
DMSO
AU-15330
0 24 48 0 24 48 (h)
PARP
Cleaved-PARP
β-Actin

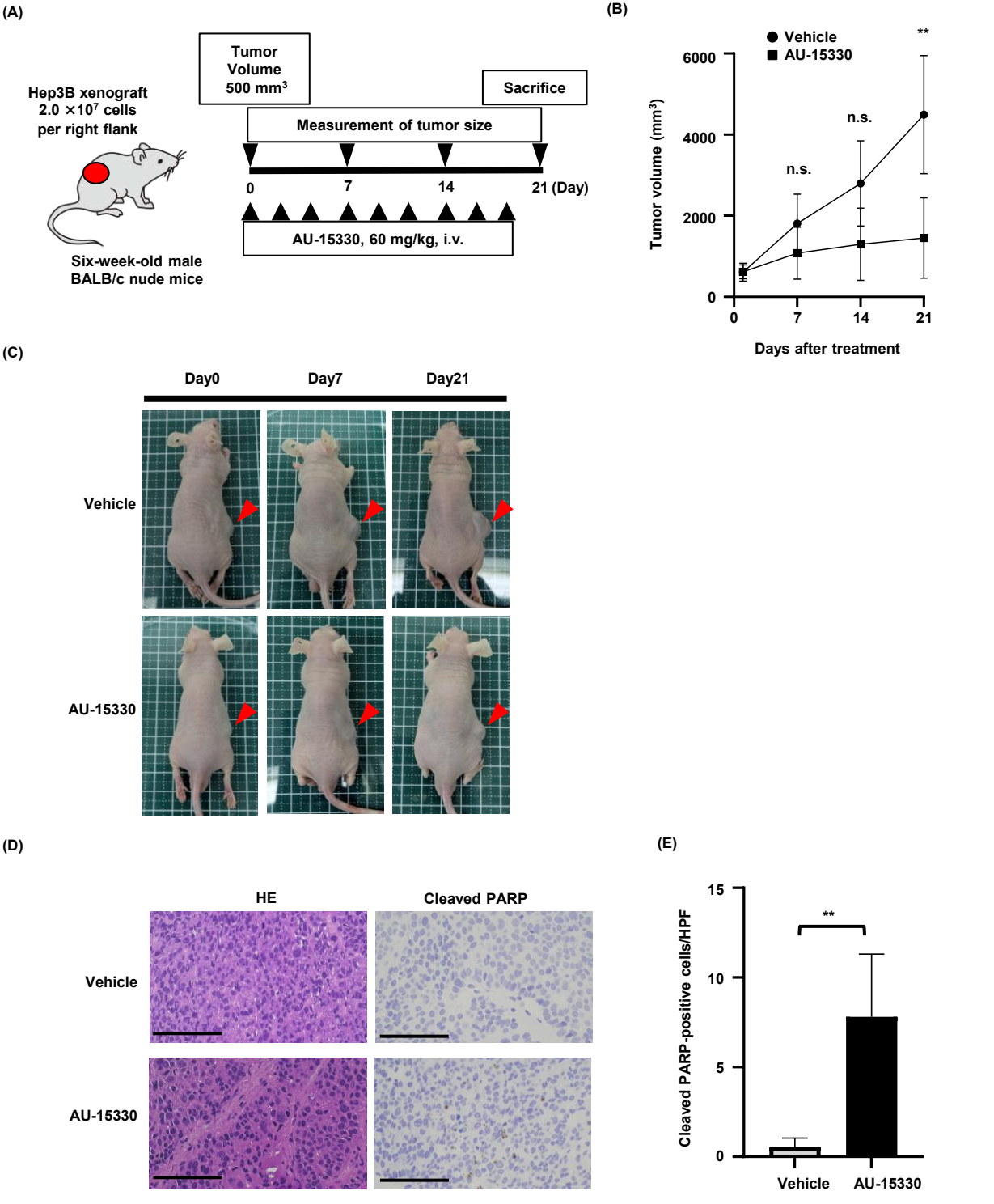
(A)
Tumor Volume 500 mm3
Sacrifice
Hep3B xenograft 2.0 ×10^7 cells per right flank
Measurement of tumor size
0
7
14
21 (Day)
AU-15330, 60 mg/kg, i.v.
Six-week-old male BALB/c nude mice
(B)
Vehicle
AU-15330
**
n.s.
n.s.
Tumor volume (mm3)
6000
4000
2000
0
0
7
14
21
Days after treatment
(C)
Day0
Day7
Day21
Vehicle
AU-15330
(D)
HE
Cleaved PARP
Vehicle
AU-15330
(E)
Cleaved PARP-positive cells/HPF
15
10
5
0
**
Vehicle
AU-15330

(A)

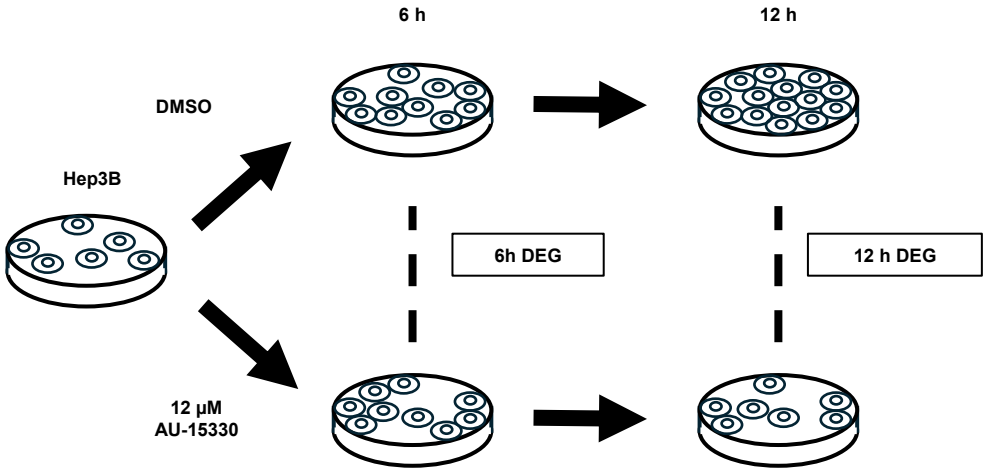


(B)

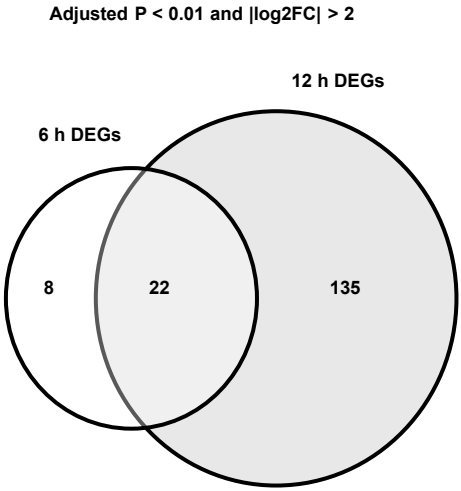


(C)

| Gene | Log2FoldChange 6 h | 12 h | Δ12 h-6 h |
|---|---|---|---|
| PTX3 | -3.125 | -3.022 | 0.103 |
| PLAU | -2.846 | -3.359 | -0.514 |
| TGILR | -2.842 | -3.844 | -1.002 |
| ISX | -2.804 | -4.591 | -1.788 |
| C10orf55 | -2.737 | -3.147 | -0.410 |
| ANKRD1 | -2.670 | -2.587 | 0.083 |
| CCR6 | -2.530 | -3.277 | -0.748 |
| DEPP1 | -2.517 | -2.977 | -0.460 |
| IRF8 | -2.511 | -2.492 | 0.019 |
| LOC105376222 | -2.494 | -3.993 | -1.498 |
| GPAM | -2.435 | -5.112 | -2.677 |
| SLC2A14 | -2.430 | -2.571 | -0.141 |
| B3GNT3 | -2.366 | -4.815 | -2.449 |
| SPSB4 | -2.265 | -3.064 | -0.799 |
| ANKS4B | -2.228 | -2.577 | -0.350 |
| GCNT3 | -2.091 | -3.657 | -1.566 |
| HS1BP3-IT1 | -2.074 | -2.899 | -0.825 |
| GDA | -2.025 | -2.426 | -0.401 |
| BAAT | -2.022 | -3.042 | -1.020 |
| FOXJ1 | -2.015 | -3.137 | -1.122 |
| NEURL1B | -2.006 | -2.525 | -0.520 |
| CHAC1 | 2.486 | 2.293 | -0.193 |



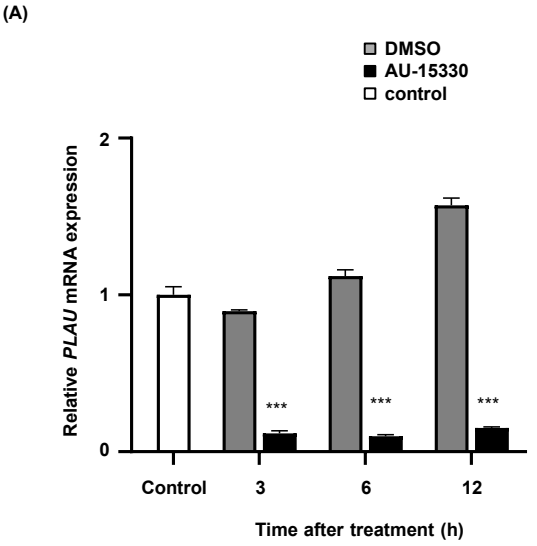
(A)
DMSO
AU-15330
control
Relative PLAU mRNA expression
2
1
0
***
***
***
Control
3
6
12
Time after treatment (h)

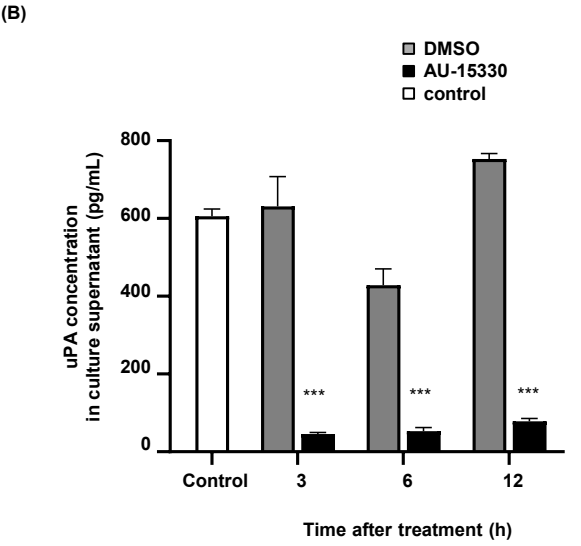
(B)
DMSO
AU-15330
control
uPA concentration in culture supernatant (pg/mL)
800
600
400
200
0
***
***
***
Control
3
6
12
Time after treatment (h)

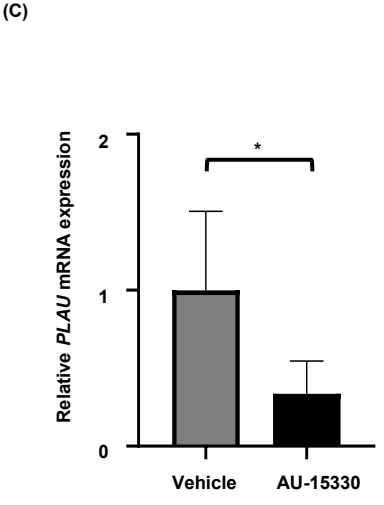
(C)
Relative PLAU mRNA expression
2
1
0
*
Vehicle
AU-15330

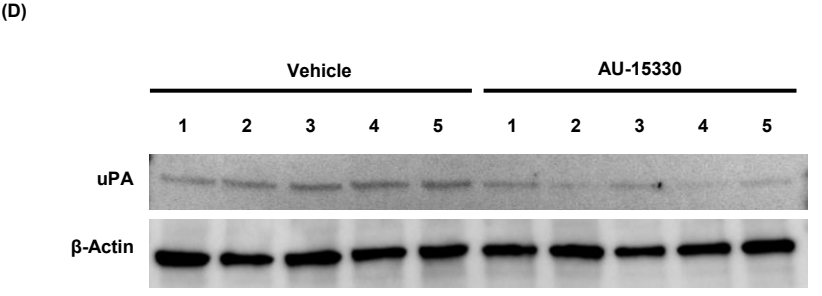
(D)
Vehicle
AU-15330
1
2
3
4
5
1
2
3
4
5
uPA
β-Actin

(A)

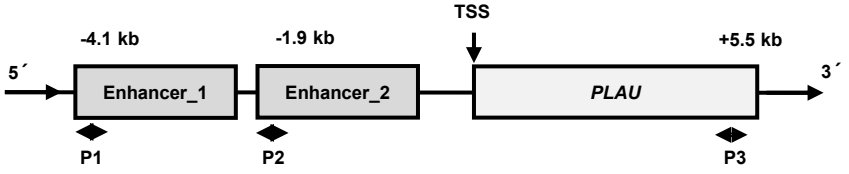
TSS
-4.1 kb
-1.9 kb
+5.5 kb
5´
Enhancer_1
Enhancer_2
PLAU
3´
P1
P2
P3

(B)

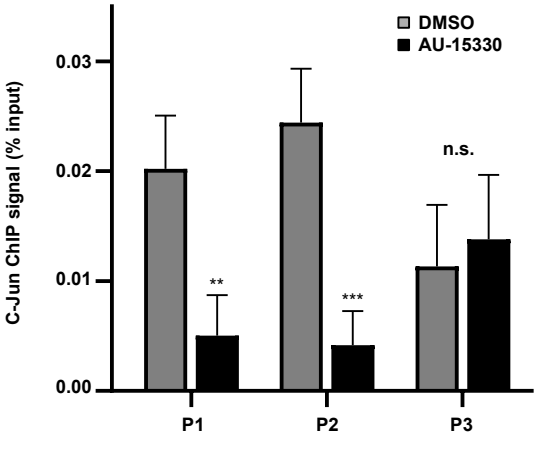
DMSO
AU-15330
C-Jun ChIP signal (% input)
0.03
0.02
0.01
0.00
**
***
n.s.
P1
P2
P3

(C)

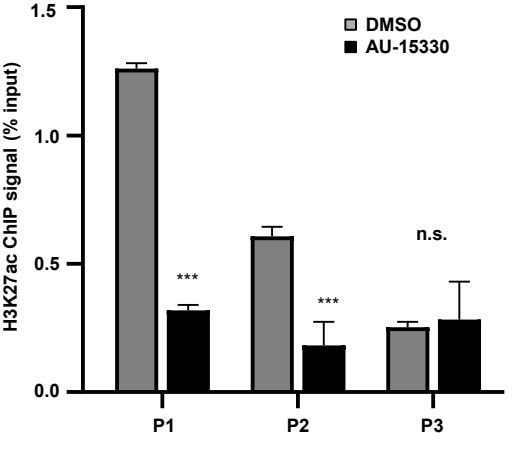
DMSO
AU-15330
H3K27ac ChIP signal (% input)
1.5
1.0
0.5
0.0
***
***
n.s.
P1
P2
P3

(D)

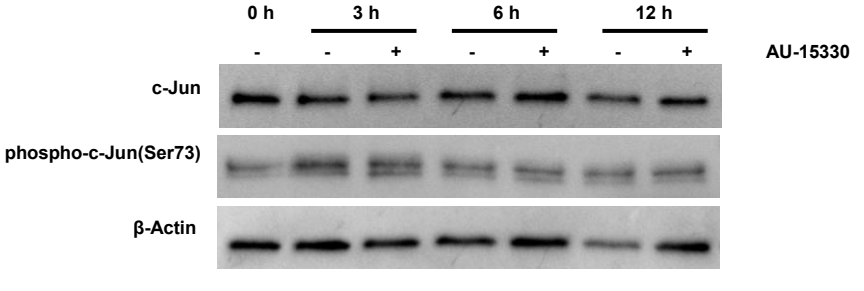
0 h
3 h
6 h
12 h
- - + - + - +
AU-15330
c-Jun
phospho-c-Jun(Ser73)
β-Actin

(A)

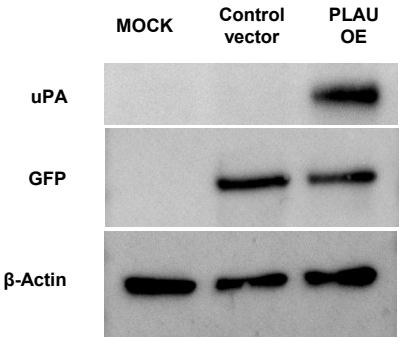


(B)

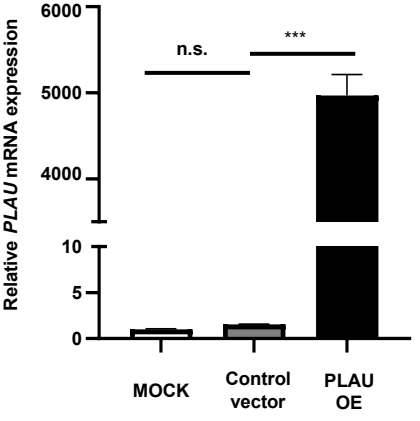


(C)

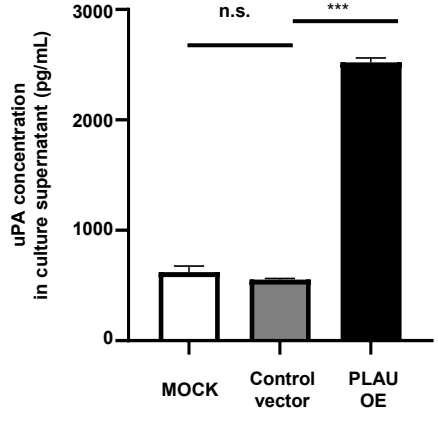


(D)

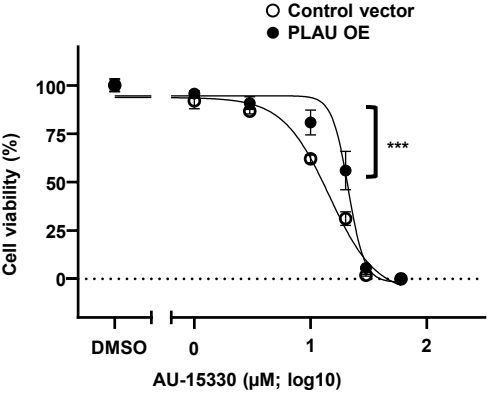


Control vector : $IC_{50}$ = 12.1 μM
PLAU OE : $IC_{50}$ = 19.5 μM

## Supplementary Files

This is a list of supplementary files associated with this preprint. Click to download.

- FigureS15.pdf